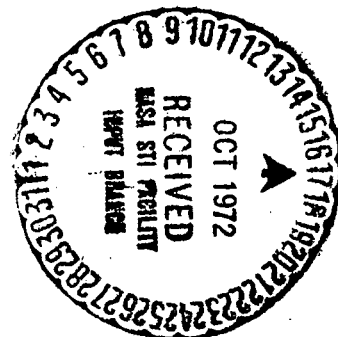EVOLUTION WITH NEUTRINO LOSSES AND THERMAL PULSES
OF THE HELIUM-SHELL SOURCE IN A STAR OF 5 SOLAR
MASSES

A. Weigert

.Stellar Evolution VI.

Evolution with Neutrino Losses and Thermal Pulses of the

Helium-Shell Source in a Star of 5 Solar Masses[*].

A. Weigert

The core contraction after the central helium burning is

recalculated for a 5 $M_{\odot}$-star. Energy losses due to photo-

neutrinos and plasma neutrinos are now taken into account.

When these losses become larger than the energy released by

the contraction, the central temperature begins to decrease

before the ignition temperature of carbon burning is

reached. The neutrino luminosity of the models remains

small. - A local thermal instability appeared in the

helium burning shell source of the models. The resulting

thermal runaway was followed numerically. After a rapid

increase in temperature and a rapid expansion, the

region of the shell source becomes stable; then it

_____

* Thesis for Habilitation as Docent, Göttingen 1966

slowly contracts until it is again unstable and so on. Six of the "thermal pulses" of the shell source are calculated. They appear with growing amplitude in time intervals of some 10^3 years.

1. Introduction

The present calculations were originally undertaken to show how strong neutrino emission can influence the evolution of stars of mean masses. Subsequently a thermal instability of the helium shell source appeared unexpectedly in the models. As a result of that the interest was also focussed on the events in the star, namely the thermal pulses caused by this instability.

Generalizations of a modern theory of weak interactions (theory of universal Fermi-interaction) led to the assumption that there is a series of processes during which large quantities of neutrinos are formed under the conditions in the interior of the star (cf. review e.g. by Chiu and Reeves). It has been pointed out repeatedly that it might perhaps be possible to gain an insight into the existence or nonexistence of these postulated processes from astrophysical studies. Conclusions to that effect appear possible in principle if one considers the time scales of certain phases of stellar evolution: due to their small

effective cross section, neutrinos are capable of transporting energy in an unimpaired fashion out of the star thus adding to the luminosity of a star the "neutrino luminosity" which has to be taken into consideration as loss in energy of the system. For a given energy supply which is released in the interior of the star in the phase under consideration the duration of this phase of stellar evolution will thus be reduced. Theoretically, this should reduce the expected abundance of stars of the corresponding type and a comparison with the observation should be possible. (Cf. for instance, the discussion in Hyashi, Hoshi, Sugimoto, 1962, for the phase of carbon-burning in red giant stars of open star clusters.)

Here, not only the unequivocal correlation of these (late) theoretical evolutionary phases with certain observed types of stars is problematic. The reliable calculation of the neutrino luminosities to be expected is also difficult. For this purpose one frequently finds in the literature temperature and density values used from star models which had been calculated without neutrino losses. The neutrino luminosity thus calculated is frequently comparable with the

photoluminosity of the models. Naturally, this does not answer the question whether similar stellar models would have been obtained at all had a strong neutrino emission been taken into consideration.

It can be expected from the dependence of the released neutrino energy from temperature and density, that this energy loss in stars of mean masses will only become significant after the helium burning. (The formulae used for the neutrino losses are given in Chapter 2). The next central burning in these stars is the carbon-burning.

Deinzer and Salpeter (1965) calculated for this phase strongly simplified models which took the neutrino losses into consideration. However, the question remains still unanswered, how the stars arrive at this state. How can the time-dependent problem be solved with realistic initial values? What are the evolutionary phases of stars after the termination of helium burning (where neutrinos do not play a role) and at the beginning of considerable neutrino losses. In order to study the effect of the neutrinos, this phase of core contraction must under otherwise identical conditions first be calculated without and then with neutrino emission. Suitable comparative calculations without neutrino losses for the entire phase inclusive of the

carbon flash are available, namely for a star of M = 5 M$_\odot$ of

the population I (X$_{outside}$ = 0.602, Z = 0.044). (cf. Kippenhahn,

T$_\text{h}$omas, Weigert, Stellar Evolution IV and V, 1965 and 1966; in

the following cited as KTW IV and KTW V.)

These calculations have now been repeated with neutrino

losses but otherwise with the same computer program, with the

same opacity values and starting from the same original models.

The results are described in Chapter 3. Upon contraction of the

exhausted carbon-oxygen-core the density and the temperature

in the center begin to increase. The behavior of the central

region changes if in the course of this event the neutrino

losses become greater than the energy released by the thermo-

dynamic change of state: upon further contraction the central

temperature decreases. It drops finally even below the value

which it had during helium burning. The models have their

maximum of temperature in the helium-burning shell source.

The "neutrino luminosity" (originating predominantly from the

exhausted core) decreases again slowly but reaches never a value

of more than a few percent of the outside luminosity. The stellar

models are thus preventing the density and temperature regions

of high neutrino emission. This indicates that small neutrino

losses may also strongly influence the overall evolution once

they become significant in partial regions of the star for the

local energy balance.

- 6 -

The outer convective zone penetrates simultaneously the interior of the star; hydrogen is transferred to the interior, helium to the outer regions. (The He-content of the outer layers increases by approximately 5%). As soon as the helium shell source approaches from the interior, a second hydrogen-burning begins in one of the shell sources. The entire luminosity will soon be taken over to the extent of 90% by this hydrogen-burning. The productivity of the helium source decreases correspondingly. This is easily understandable from the fact that the helium reactions take place at considerably higher temperature but have an approximately ten-fold smaller yield of energy per gram as compared with the hydrogen reactions. (These events are discussed in Chapter 4.)

While in the models calculated thus far the carbon flash had been prevented by the cooling action of the neutrino losses, in the last models a new phenomenon occurred which is similar to that of the flash: thermal instabilities occur in the helium shell source which after revitalization of the hydrogen source seemed to be degraded to complete insignificance. These local instabilities were discovered at approximately the same time by Schwarzschild and Härm (1965) in quite different stars, initially (like here) by numerical difficulties then with the help of a linear perturbation calculation.

The events caused by the instability in the star under
discussion could only be studied by the solution of the entire
system of nonlinear equations. These events are described in
Chapter 5 as thermal pulses of the helium shell source. The
temperature in this shell source increases very rapidly during
the pulse and brings about extensive energy production. (The
excess of energy can not be dissipated by work of expansion
and is converted to inner energy.) Locally the luminosity
increases very strongly (temporarily to a multiple of the
outside luminosity.) This is accompanied by the formation of a
convective shell which approaches the hydrogen-rich outer regions.
The shell source moves eventually out of this unstable situation
by expansion. A subsequent contraction which, last not least,
is caused by the hydrogen-shell source above induces new instability.
The thermal pulses are thus repeating themselves, namely in
intervals of some 10^3 years. The amplitudes are steadily
increasing. A total of six of this type of pulses were
calculated. This required extremely small time steps and,
as a result of that, the calculation of very many models.

The treatment of the numerical difficulties which were
encountered in connection with the extremely thin hydrogen shell
source and the thermal pulses is discussed in the appendix.

A preliminary account of the numerical discovery of the thermal

pulses has already been presented at the meeting of the

Astronomical Society (Weigert, 1965).

The calculations were carried out with the computer IBM 7090

at the Institute for Plasmaphysics, Garching.

2. The Formulae for the Neutrino Losses

The system of differential equations and its treatment

by the computer program have been described in detail by

Hofmeister, Kippenhahn, Weigert (1964 and 1966). The law of

conservation of energy had to be changed and is now programmed

in this form

$$\frac{\partial L_r}{\partial M_r} = \epsilon + \epsilon_g - \epsilon_\nu \tag{1}$$

with $\epsilon_\nu > 0$. (As usual, M_r designates the mass of the sphere

with the radius r around the center of the star, L_r the energy

which in one second flows through its surface to the outside;

ϵ is the energy production rate per second and per gram of

stellar matter by nuclear reactions, here $\epsilon = \epsilon_H + \epsilon_{He} + \epsilon_C$;

$\epsilon_g = -T \frac{\partial S}{\partial t}$ is the energy which is released upon the thermo-

dynamic change of state per gram and second).

The term ϵ_ν which has been added in equation (1) is the energy which goes - per second and per gram of stellar matter - into the neutrinos. Only two processes are of interest for the range of density and temperature in question, namely the formation of photoneutrinos ($\gamma + e^- \rightarrow e^- + \nu + \bar{\nu}$) and of plasma neutrinos (plasmon $\rightarrow \nu + \bar{\nu}$). Formulae for the ϵ_ν-values of these processes can be found in the publications of Adams, Ruderman, Woo (1963), Chiu (1961), Inman and Ruderman (1964) as well as in the already cited review of Reeves. The ϵ_ν-values of Inman and Ruderman (1964) have been calculated and tabulated for plasma neutrinos. A very good approximation of these values can be obtained for all regions with the formula

$$\epsilon_{Pl} = \frac{\epsilon_1}{1 + e^{\Phi - 1/\Phi}} + \frac{\epsilon_2}{1 + e^{-\Phi + 1/\Phi}} , \qquad (2)$$

which interpolates between the two approximations

$$\epsilon_1 = 5.55 \cdot 10^{-10} \cdot \varrho^2 \, T_8^3 \cdot (1 + 6.35 \cdot 10^{-5} \cdot \varrho^{2/3})^{-3/2} \, \text{erg g}^{-1} \, \text{sec}^{-1} \qquad (3)$$

for $\Phi \leqslant 1$, and

$$\epsilon_2 = 3.16 \cdot 10^{-14} \cdot \varrho^{2.75} \, T_8^{1.5} \cdot (1 + 6.35 \cdot 10^{-5} \cdot \varrho^{2/3})^{-15/8} \cdot e^{-\Phi} \, \text{erg g}^{-1} \, \text{sec}^{-1} \qquad (4)$$

for $\Phi \gg 1$.

Here are $T_8 = T \cdot 10^{-8}$ and

$$\Phi = \frac{\hbar \, \omega_{Pl}}{kT} = 3.34 \cdot 10^{-3} \frac{(\varrho/\mu_e)^{1/3}}{T_8} \cdot \left[1 + 1.01 \cdot 10^{-4} \cdot \left(\frac{\varrho}{\mu_e}\right)^{2/3}\right]^{-1/4}. \qquad (5)$$

ω_{Pl} is the plasma frequency and μ_e the mean molecular weight per free electron. (For T = const. we obtain according to equation (2) a maximum of ϵ_{Pl} at $\Phi \approx 5$, thus for $\bar{h} \, \omega_{Pl} \approx 5$ kT.)

For the photoneutrinos in nondegenerate matter the following is valid:

$$\varepsilon_{Ph} = 1.67 \cdot \mu_e^{-1} \cdot T_8^8 \; \text{erg g}^{-1} \text{sec}^{-1}. \qquad (6)$$

This was set for $G = \lg T - \frac{2}{3} \lg \varrho - 5.25 \geqq 0$ and corresponds approximately to degeneracy parameters $\Psi \leqq 0$. With increasing degeneracy the electron finds upon impuls changes fewer free cells of the phase space and ϵ_{Ph} will therefore become smaller and smaller. Equation (6) was also used for $G < 0$ with an additional reduction factor F on the right-hand side, whereby ln F = 5G. (This again is only an interpolation formula; it corresponds approximately to the lines ϵ_{Ph} = const. found with Reeves, 1966, Fig. 2; in the ρ,T-region which is of interest here, it plays, however, only a role in a very small interval or non at all.)

We then wrote

$$\epsilon_r = \epsilon_{Pl} + \epsilon_{Ph}. \tag{7}$$

It must be emphasized that there it was only important to program a steady formula for ϵ_ν which reflected the approximate dependence of ρ, T but not high accuracy. The resulting curves ϵ_ν = const. are represented in Fig. 1. In this Fig. 1, the curve is also represented on which $-\epsilon_\nu + \epsilon_c / X_c^2 / c = 0$ (ϵ_C is the energy production rate, f_C is the shield factor for the $C^{12} + C^{12}$ -reaction; X_C is the C^{12} -abundance). For $X_C^2 \cdot f_C = 1$, we find $\epsilon_C - \epsilon_\nu < 0$ below this curve, and $\epsilon_C - \epsilon_\nu > 0$. Due to the strong T-dependence of ϵ_C the carbon-burning starts in each case in the immediate vicinity of this curve. The central values of density and temperature for the 5 $M_\odot$-star are also plotted to the point of termination of the center helium-burning (up to model 313 in KTW IV). As the temperature increases to the point of carbon-burning, the central region of this star must certainly pass through a region with negative energy balance ($\partial L_r / \partial M_r < 0$, equation (1)), since the values of ϵ_g found upon contraction are from experience lower than 10^5 erg/g sec.
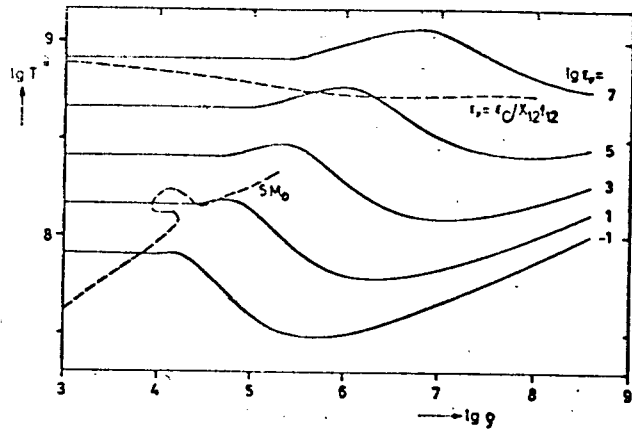
Figure 1. The curves ϵ_ν = const. in the $\log_\rho$ - log T-diagram.
To the left in the diagram the photoneutrinos are predominant
(straight lines parallel to the abscissa), to the right the
plasma neutrinos. On the upper dashed curve ϵ_ν is equal to the
energy production due to C^{12}-C^{12}-burning. Furthermore, the
sequence is shown which the center of the 5 $M_\odot$-star followed
in this diagram before it disappeared in the center of the
helium content (according to calculations in KTW IV).

3. Results of the Calculations with Neutrino Losses

Table 1 summarizes the sequence of 317 models which was calculated for this purpose in dependence of time. The onset was made to coincide with Model 290 of the evolutionary sequence for 5 solar masses, which was calculated without neutrino effects, (KTW IV). In the HR-diagram this Model 290 is located on the second large loop to the left in the region of the super giants (cf. KTW IV, Fig. 1 between G and H). As in the earlier calculations the evolutionary sequenc goes first to the left (up to Model 298) then to the right and beginning with Model 304 with increasing luminosity it proceeds in an upward direction close to the track of fully convective models. From Model 400 through 408 the direction is reversed for a short distance before it proceeds upwards again (cf. Chapter 4 and KTW V). The significant events in the interior of the star, to be described here, take place after Model 303, i.e., during the time during which the star moves along the track of fully convective models in the HR-diagram.

In the original Model 290 the central helium-burning has not yet been fully completed. In the center we have a helium content of $Y = 0.0064$, the energy balance is maintained to about equal parts by helium-burning ($\epsilon_{He} = 64$ erg g^{-1} sec^{-1})

Table 1. Coordinates in the H-R-diagram and age (in 10^7 years) of several models. $X_{\text{illegible}}$ is the hydrogen abundance of the outer layers, L_H/L the contribution of the hydrogen-shell source to the total luminosity.

1 Modell Nr.	2 Alter	$\log \dfrac{L}{L_\odot}$	$\log T_e$	X_e	$\dfrac{L_H}{L}$
290	7.583	3.255	3.682	0.602	0
298	7.814	3.283	3.762	0.602	0
301	7.849	3.228	3.686	0.602	0
303	7.853	3.152	3.648	0.602	0
313	7.895	3.437	3.599	0.602	0
314	7.910	3.516	3.590	0.602	0
319	7.947	3.816	3.553	0.601	0
320	7.948	3.828	3.551	0.600	0
323	7.950	3.868	3.545	0.574	0
331	7.951	3.864	3.545	0.563	0
340	7.951	3.883	3.544	0.562	0
350	7.956	3.980	3.536	0.559	0
400	7.966	4.164	3.512	0.556	0
408	7.969	4.084	3.522	0.556	0.04
411	7.970	4.218	3.504	0.556	0.67
430	7.970	4.223	3.503	0.556	0.73
500	7.971	4.263	3.499	0.556	0.82
606	7.973	4.310	3.485	0.556	0.92

1 Model Nr.; 2 Age

and by contraction (ϵ_g = 50 erg g^{-1} sec^{-1}). Compared with the sum of both terms the energy losses by neutrinos in the center (ϵ_ν = 14 erg g^{-1} sec^{-1}) are still small. (This was a pre-requisite according to which the original model for the comparative calculation had been selected.) The energy loss per second due to neutrinos for the entire star ("neutrino luminosity" L_ν) was found by integration to be

$$L_\nu = \int_0^M \epsilon_\nu \, dM_r = 3.1 \, L_\odot \, ,$$

it thus is negligible against the optical luminosity of $10^{3.2} \, L_o$ (cf. Table 2). According to that there are practically no changes in the initial models as compared with those without neutrino effects. The energy of Model 290 which goes into neutrinos, originates almost entirely from helium-burning: ϵ_g and ϵ_ν are changing only slowly from the center to the outside while ϵ_{He} increases rapidly and strongly (due to increasing Y).

In the following models the same event takes place in the vicinity of the center as was the case in earlier calculations. The helium content disappears in a mass region which increases from the center towards the outside: it is Y = 0 in the center from Model 311 on, for M_r/M = 0.015 from

Table 2. The "neutrino luminosity" L_ν and the central values
of ε_{He}, ε_g and ε_ν (all in erg g^{-1} sec^{-1}) for several models

Modell Nr.	$L_\nu/L_\odot$	L_ν/L	ε_{He}	ε_g	ε_ν
290	3.1	0.0017	$6.4 \cdot 10^1$	$5.0 \cdot 10^1$	$4.4 \cdot 10^1$
301	17.1	0.010	$3.2 \cdot 10^1$	$1.5 \cdot 10^2$	$1.1 \cdot 10^2$
314	76.7	0.023	0	$4.7 \cdot 10^2$	$8.4 \cdot 10^2$
319	395	0.060	0	$6.8 \cdot 10^2$	$1.6 \cdot 10^3$
331	479	0.065	0	$6.4 \cdot 10^2$	$1.5 \cdot 10^3$
400	586	0.040	0	$2.7 \cdot 10^2$	$5.0 \cdot 10^2$
430	450	0.027	0	$1.8 \cdot 10^2$	$3.4 \cdot 10^2$

Model 314 on, for $M_r/M = 0.11$ from Model 331 on. Thus a
helium shell source has been formed which is burning more and
more to the outside. The exhausted central region within it
contracts whereby the central temperature initially increases
further (Fig.2). In this contracting central region ε_g
increases also; it is already considerably larger than ε_{He},
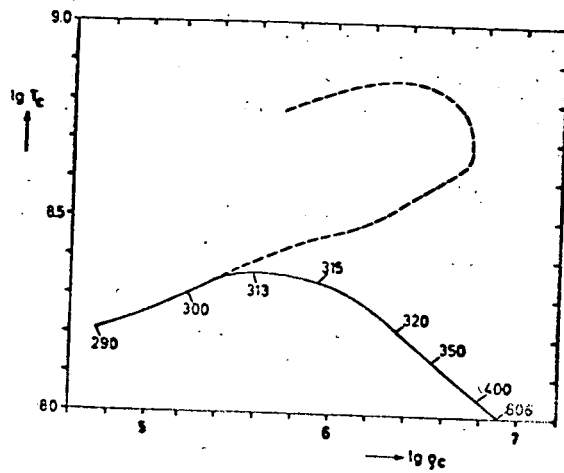before $Y = 0$ (cf. Table 2, Model 301).

Figure 2. Central values of density and temperature during the evolution. The model numbers given show the correlations with Table 1. The dashed curve indicates the sequence which resulted without taking into consideration the neutrino losses (cf. KTW V; the steep slope of this curve represents the carbon-flash).

With increasing central temperature the energy going
into neutrinos increases, however, also steadily (Table 2).
In the center of Model 311, ϵ_ν becomes approximately as large
as ϵ_g, in the following models even larger than ϵ_g and thus
the energy balance in the center becomes negative for the
first time ($\epsilon_g - \epsilon_\nu < 0$, thus $\partial L_r / \partial M_r < 0$, since we have
already $\epsilon_{He} = 0$). The effects of the neutrino losses on
the subsequent evolution are now considerable and clearly
distinguishable in the models. The central temperature
reaches with log $T_c + 8.357$ a maximum for Model 313 and begins
from thereon to decrease slowly, subsequently more rapidly
(Fig. 2 and 3a). The central density increases, however,
further (the contraction is still going on); the slope in the
ρ_c-T_c-diagram has approximately the same value, only the
reversed sign as before. Due to the neutrino losses the increase
in central temperature is prohibited until the point of ignition
of carbon-burning has been reached (lgT $\approx$ 8.6). In several
time steps after Model 313 the temperature continued to increase
in a shell around the center. Thus it does not seem to be ex-
cluded that the carbon-flash may start in a spherical shell
around the center. This may also be the case for other models
(for instance with other masses). Here, finally, the temperature
began to decrease in the entire exhausted core as soon as ϵ_ν, also
in some distance from the center, began to become greater than ϵ_g.

Since the decrease in temperature results in a decrease in neutrino losses one can say: the entire center region of the star adjusts itself in such a way that extremely high neutrino losses are prevented (cf. in Table 2 the decrease of L_ν after Model 400).

The models assume thus in the central region a completely different unusual structure. The maximum of temperature is with approximately $2.7 \cdot 10^8$ °K located in the helium-burning shell source in which the entire amount of luminosity is produced which is dissipated to the outside. From the inner edge of this shell source on the temperature decreases toward the center, i.e. there is a flux of energy directed toward the center ($L_r < 0$) where it is converted into neutrino energy and transported out of the star by the neutrinos. Details on the structure of this model can be found in Table 3 in which Model 400 is represented. The luminosity which is directed to the interior is admittedly smaller in its absolute amount than the outside luminosity ($L_r \gtrless -0.015L$), however, quite considerably by comparison with the luminosity of the sun ($L_r \gtrless -0.015L = -220L_0$). It is the result of strong degeneracy that such an amount of energy can be transported in this exhausted core with a low temperature gradient (from $M_r/M = 0.14$ to the center T decreases only by a factor of 2.4 while P increases by more than 2 powers of 10). The degeneracy parameter

Table 3. Model Nr. 400. In the convective regions log T is printed in italics. ε (nuclear energy production), ϵ_g and ϵ_ν are given in erg g^{-1} sec^{-1}.

M_r/M	$\log P$	$\log T$	$\log \rho$	L_r/L	Y	$\epsilon \cdot 10^{-4}$	$\epsilon_g \cdot 10^{-3}$	$\epsilon_\nu \cdot 10^{-3}$
0.9710	4.61	*4.189*	—7.665	1.0000	0.400	0	0.0	0
.8799	5.38	*4.495*	—7.195	1.0000	0.400	0	0.0	0
.7720	5.81	*4.657*	—6.939	1.0000	0.400	0	0.0	0
.6557	6.12	*4.776*	—6.747	1.0000	0.400	0	0.0	0
.5524	6.35	*4.862*	—6.603	1.0000	0.400	0	0.0	0
.4720	6.52	*4.925*	—6.498	1.0000	0.400	0	0.0	0
.3884	6.71	*4.991*	—6.384	1.0000	0.400	0	0.0	0
.3000	6.93	*5.071*	—6.243	1.0000	0.400	0	0.0	0
.2255	7.22	*5.170*	—6.063	1.0000	0.400	0	0.0	0
.1649	8.29	*5.517*	—5.375	1.0000	0.400	0	0.0	0
.1600	9.74	*5.942*	—4.413	1.0000	0.400	0	0.0	0
.1595	10.67	*6.199*	—3.783	1.0000	0.400	0	0.0	0
.1592	11.65	*6.462*	—3.112	1.0000	0.400	0	0.0	0
.1591	12.48	*6.681*	—2.539	1.0000	0.400	0	0.0	0
.1591	13.38	6.907	—1.869	1.0000	0.400	0	1.8	0
.1590	13.89	7.035	—1.480	0.9999	0.400	0	3.0	0
.1590	14.58	7.180	—0.588	0.9999	0.956	0	2.8	0
.1589	15.35	7.360	0.038	0.9998	0.956	0	5.8	0.00
.1586	16.21	7.571	0.684	0.9996	0.956	0	4.0	0.00
.1582	17.03	7.782	1.289	0.9992	0.956	0	7.5	0.00
.1575	17.88	7.990	1.945	0.9976	0.956	0	23.6	0.00
.1569	18.47	8.133	2.399	0.9953	0.956	0	18.2	0.01
.1565	18.86	8.230	2.681	0.9933	0.956	0.13	21.0	0.03
.1561	19.15	8.303	2.907	0.9330	0.905	5.28	33.2	0.13
.1559	19.27	8.329	3.039	0.7137	0.735	11.30	52.3	0.22
.1559	19.32	8.337	3.098	0.5693	0.633	12.70	69.6	0.25
.1557	19.42	8.348	3.230	0.3095	0.386	7.34	98.8	0.30
.1556	19.54	8.355	3.389	0.1501	0.192	2.30	104.0	0.34
.1541	20.19	8.374	4.095	0.0298	0.013	0.03	30.7	0.49
.1498	20.93	8.401	4.796	0.0107	0.001	0.00	10.3	0.64
.1410	21.55	8.417	5.315	—0.0013	0.000	0	5.6	0.44
.1063	22.44	8.357	5.983	—0.0151	0.	0	1.9	1.86
.0615	22.99	8.244	6.359	—0.0088	0	0	0.8	2.07
.0254	23.32	8.140	6.588	—0.0023	0	0	0.5	1.22
.0084	23.49	8.085	6.702	—0.0005	0	0	0.3	0.78
0	23.63	8.045	6.793	0	0	0	0.3	0.50

of this center is $\Psi = 41$). In the entire core, heat conductivity
by the degenerate electron gas dominates already over radiative
transport. The effective $\varkappa$-values are between 10^{-2} and 10^{-4}.

As can be seen from Table 2, energy which goes into neutrinos
(L_ν), is still increasing when, due to cooling of the center,
ε_ν has already decreased there. The maximum of L_ν with
approximately $L_\nu \approx 590\ L_\odot$ is near Model 400. Due to the
simultaneous strong increase in outside luminosity, the
maximum of L_ν/L is already to be found earlier (6.5% in Model 331).
In any event, the "neutrino luminosity" remains small by
comparison with the optical luminosity over the entire period
of time covered by these calculations. L_ν is produced almost
exclusively by plasma neutrinos, the contribution by photoneutrinos
is negligible. A comparison of the ρ- and T-values of Table 3
shows that the core region ($M_r/M \lessapprox 0.14$) is to a considerable
extent in that region of Fig. 1, where the curves $\varepsilon_\nu = $ const.
are progressing from the upper left to the lower right $\left[\Phi < 1 \right.$
in equation (2) through (5)$\left.\right]$ .In Models 331 and 400 93% and 97%,
respectively, of L_ν are produced in the exhausted core (for
$M_r/M \lessapprox 0.11$ and $\lessapprox 0.14$, respectively). This energy is covered
by contraction of these regions of the core thus resulting in a
large positive ε_g, primarely in the outer regions (cf. Table 3).

The changes in central temperature T_c and outside luminosity L in dependence of time are shown in Fig. 3a and b and are compared with the corresponding changes without neutrino effects (KTW IV and V). The two curves for T_c are identical from the beginning of the calculation (in Fig. 3 not shown) up to the age of $7.87 \cdot 10^7$ years (Model 311). They begin to diverge when ϵ_ν in the center becomes comparable with ϵ_g. Following Model 390 (age = $7.962 \cdot 10^7$ years) the decrease in T_c is again noticably slower. Whether this indicates the onset of a new evolutionary phase in which the central temperature is constant with time, can not be decided from the present calculations. Such tendency might be expected from the stability consideration in KTW V where thermal stability had been found for "negative energy production" $(\frac{\partial L_r}{\partial M_r} - \epsilon_g < 0)$.

In Fig. 3b the minimum of L appears somewhat earlier than in the previous calculations. The reason for that is propably the selection of somewhat too large time steps in this initial phase. What is actually of interest, is the subsequent rate with which the star is strongly increasing its luminosity while moving upward in the HR-diagram along the track of fully convective models. Up to Model 313 this rate is also approximately the same like that of cases without

neutrino losses. Thereafter the increase becomes again more
rapid than in the comparative calculations. This indicates
once more how the evolution of the outer layer is directed by
the central region (only there occur considerable energy
losses due to neutrinos). From this effect one can at the
same time see how wrong conclusions can be drawn on the
length of a certain evolutionary phase if one resorts to models
without neutrino losses and applies only one energy balance
for the entire star. If during the computation of the age one
wants to forego the calculation of evolutionary sequences one
must at least be certain that the energy balance in individual
mass regions of the star is not disturbed considerably by
neutrino losses. This may, in particular, be the case in the
central region of shell source models. For instance, one
obtains in Model 400 for the boundary of the exhausted core
$(\epsilon_{He} = 0$ for $M_r \leqq M_1 = 0.14$ M)

$$L_g = \int_0^{M_1} \epsilon_g \, dM_r = 546 \, L_\odot \, , \quad L_r' = \int_0^{M_1} \epsilon_r \, dM_r = 566 \, L_\odot$$

and $L_r = -20 \, L_\odot$. In an approximation we thus have $L_\nu^\circ \simeq L_g$;
the neutrino losses are considerable for the energy balance
of the core regions, despite the fact that they are negligible
in the energy balance of the entire star $(L_\nu^\circ \simeq 0.04 \, L)$.
Naturally, no conclusions shall be drawn, for instance on the

observed frequency of certain types of stars from the changes

in rate in the phase discussed here, which is short in any

event.

It would, however, be extremely important to know the

evolution (particularly of the central region) in the subsequent

phases. The fact that the central density continues to increase

strongly upon cooling, leaves open two entirely different

explanations. In the ρ_c-T_c-diagram the models are in the

region $\Phi > 1$ $\left[\text{equation (5)}\right]$ where the curves $\epsilon_\nu = $ const. change

direction and proceed to the upper right. The center could move

to higher temperatures along these curves. A carbon-flash would

then, however, begin at extremely high density and in all

likelihood have quite different characteristics than those

described in KTW V. It is, however, also possible that upon

continued contraction the central region comes into the

ρ_c-T_c-area where even without neutrino losses the contraction

does not lead to continued heating but to cooling. If thus, the

entire carbon burning in stars of mean masses could be prevented

by neutrino losses, the impact would be considerable on the

theories on the formation of elements with mass numbers around 20.

Only through additional calculations will it be possible to

clarify these questions. These calculations are not possible
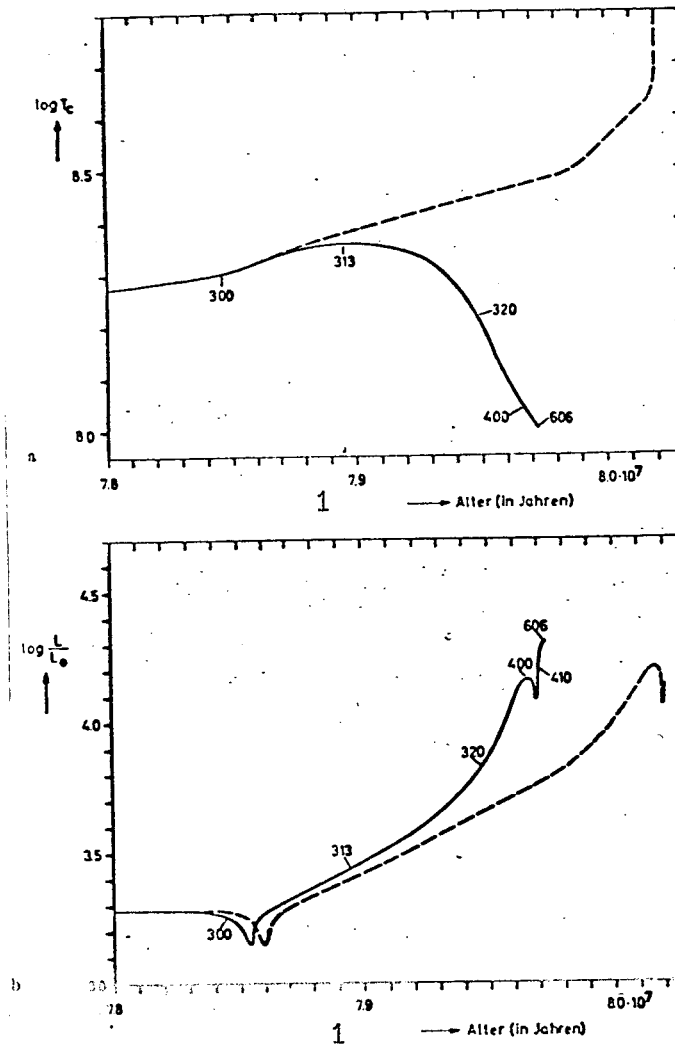
Figures 3a and b. The changes in dependence of time of the
central temperature and the luminosity of the star. The figures
given correlate the model numbers with those in Table 1. The
dashed curve is the corresponding sequence which was obtained
without consideration of neutrino losses (KTW IV and KTW V).

1 age(in years)

for the time being since in the latest models two events took place which made very small time steps a necessity and are thus delaying the calculations: the renewed occurrence of the hydrogen-shell source (cf. the following chapters).

Let us first turn to the question to what an extent the undoubtedly still present uncertainties of the formulae for ϵ_ν have an influence on the past results. M. Zaidi (1965) has found meanwhile that the formulae given in the literature for ϵ_{pl} are leading to values which are too large by a factor of 4. Corrections of such magnitude should, however, not influence the essential effect (that the central region does cool down). Fig. 1 shows that only a decrease in the ϵ_ν-values by more than 2 powers of 10 could prevent the energy balance in the center from becoming negative after the termination of helium burning.

4. The Second Hydrogen Burning

We shall now discuss the events in the layers outside of the helium burning shell source. With increasing luminosity the outer convective zone had grown to the interior. From Model 311 on it entered into a region in which hydrogen had earlier already been converted to helium. Thus, hydrogen had been mixed into these regions and helium reached the outer layer. (cf. the variation of the hydrogem content X_e of the outer layers, Table 1,

and the corresponding discussion in KTW IV). The convective

zone reached its greatest depth with Model 390 (inner boundary

at $M_r = 0.1590$). The helium content of the outer layers has in-

creased by approximately 0.05 as compared with the initial

composition.

Like in the calculations without neutrino effects the

temperature increases at the inner boundary in the region that

contains hydrogen until hydrogen-burning begins again. This

increas in temperature results from the overlapping of two

effects: initially it is the sizable effect of the penetration

of the convective boundary (and thus the mixing of hydrogen)into

regions of higher temperature; later it is the effect of the

approach of the helium-burning shell source with the temperatures

of more than 10^8 °K. With the more strongly increasing

hydrogen-burning the energy production in the helium-burning

shell source decreases continuously. The temperature decreases

here somewhat; this shell source contracts. In approximately

$7 \cdot 10^4$ years, approximately the entire energy production of

this star will be taken over by the hydrogen-burning shell

source (cf. Table 1). It is understandable that the luminosity

(L_{He}) which is produced in the helium-shell source must go back to

a maximum of approximately 1/10 of that produced in the hydrogen

shell source. Each approach of the hotter helium-shell source

causes an increase in temperature in the hydrogen shell source
and thus of the energy production. The change in distance
with time of the two sources may be described by

$$\dot{M}_H - \dot{M}_{He} = \frac{1}{X} \cdot \frac{L_B}{E_B} - \frac{1}{Y} \cdot \frac{L_{He}}{E_{He}} . \qquad (8)$$

(M_H and M_{He} are mean M_r-values for both sources, dots indicate
time derivations; E_H and E_{He} are the energies released upon
conversion of 1 g of hydrogen and helium, respectively; X and Y
indicate the weight proportions of both elements above the
corresponding source). Since $E_H/E_{He} \approx 10$, for approximately
equal X and Y, the distance of the sources will not become
smaller ($\dot{M}_H - \dot{M}_{He} \gtrless 0$) as long as $L_H/L_{He} \gtrless 10$ id fulfilled.
Only at approximately this ratio do both sources burn with
equal distance to the outside.

The renewed hydrogen-burning begins at a point where the
outer convective zone has practically produced a jump in the
chemical composition. (In the computer program this point is
treated as a genuine discontinuity which here certainly
approaches the true situation very closely.) The shell source
being formed is therefore concentrated to an extremely narrow
mass-range. This results in very high ϵ_H-values and thus very
high negative $\dot{X}$-values (because of $\dot{X} \sim -\epsilon_H$). The clean integration
in dependence of time with the method used thus far, required

therefore the calculation of many models with small time steps.)
(This was the first factor which delayed considerably the
computation of subsequent evolutionary phases.) The treatment
of this difficulty is discussed in the appendix. Almost
simultaneously with the renewed occurrence of hydrogen-burning
this star turned in the HR-diagram (Model 400). The evolutionary
sequence reversed itself (up to model 408) and moved then
again upward along the track of fully convective models (cf.
Table 1 and Fig. 3b). It is not clear, whether there is a
causative relationship between the begin of the hydrogen-burning
(in Model 400 $e_H \approx 10^{-3}$ erg g^{-1} sec^{-1}) and the change in direction
in the HR-diagram. However, both events coincided also in the
earlier calculations (KTW V), despite the fact that the models
were otherwise quite different (already beginning carbon-burning
upon neglect of the neutrinos). The models described here show
in the vicinity of the newly formed hydrogen shell source two
striking features which shall be discussed briefly. Upon outward
burning of the shell source the outer convective zone does indeed
also contract, but remains constantly in the immediate vicinity.
Its inner boundary is in the calculated models not more removed
from the range of $e_H \geqq 10^3$ erg g^{-1} sec^{-1} than $\Delta M_r \approx 10^{-4} M_\odot$. Is
there a danger that excessive convective elements do actually
penetrate the shell source, mix in new hydrogen, and transport
newly formed helium to the outside? For this purpose the ex-
pressions of the theory of "mixing length" were applied to the

inner boundary region of the convective zone in several models
from Nr. 450 to 460, in order to estimate the "overshooting"
to be expected there. (cf. Unno, 1965, for similar considerations
and expressions.) The following results were obtained in all
cases; the convective elements must be completely decellerated
after having passed a pressure difference corresponding to
$\Delta \ln P \approx 10^{-3}$ below the boundary of the convective zone which
is defined by $\bar{V}_r = \bar{V}_{ad}$. In the very narrow range of masses in
question between the convective zone and the main portion of the
shell source, the pressure increases, however, always by more
than 2 powers of 10. Mixing between the envelope and the
shell source does thus certainly not take place.

It is also striking that in the range of the hydrogen
shell source an unusually large proportion of the radiative
pressure P_R contributes to the total pressure P. Here
$\beta = 1 - P_R/P$ shows a strongly pronounced minimum which decreases
to approximately $\beta = 0.4$. As is known, small β favors the
formation of great relative amplitudes of the eigenfrequency
in pulsating stars. It would be of interest to test, whether in
these models the amplitude in the hydrogen shell source becomes
so great that the difference in energy production can induce
the frequencies (Eddington's ϵ-mechanism). If this were the
case, then one could correlate these or similar stellar models

with long-periodic variables the periods of which are of the
order of magnitude of months or years. Thus far the eigenperiod
of only one of these super giant models has been determined. It
is approximately 500 days.

5. Thermal Pulses of the Helium-Shell Source

The last models of the series described here show a
phenomenon which is similar to that of the flash: in the helium
shell source thermal instabilities are observed. These
instabilities - they are restricted to the range of a
spatially very narrow shell source in which nuclear energy
production of very high temperature exponents takes place -
were discovered recently by Schwarzschild and Härm (1965) in
stars of 1 solar mass. During a period of increasing
temperature and under certain circumstances the energy produced
can not be transferred completely; this energy is converted
to inner energy if the shell source is spatially very narrow
since under such circumstances an insufficient amount of work
of expansion is performed, the temperature increases further, etc. -
These authors determined (for a greatly simplified model) the
criteria for instability of a shell source as follows: the
decrease in temperature must be $\frac{\Delta T}{T} > \frac{4}{\nu}$ and that its extension be
$\frac{\Delta r}{r} < \frac{5}{2Q}$ (with $\nu = \frac{\partial \ln \varepsilon}{\partial \ln T}$, $Q \approx 6$). In the models of the 5 $M_{\odot}$-star
discussed, the He-shell source covered the following ranges

of temperature and radii: $8.278 \geq \lg T \geq 8.155$, $8.902 \leq \lg r \leq$

8.978 (if one considers as significant that region of the shell

source in which the energy production is $\epsilon > 10^4$ erg g^{-1} sec^{-1};

the maximum of ϵ is $1.64 \cdot 10^{-6}$.) Thus $\frac{\Delta T}{T} = 0.28$ and $\frac{\Delta r}{r} = 0.17$.

Since for the 3 α-process which is the only one considered here

the following is valid: $\nu = -3 + \frac{43.2}{T} \cdot 10^8 = 19.7...27.2$,

both conditions are fulfilled.

The linear stability theory of Schwarzschild and Härm

shows thus, for one thing, that the He-shell source is unstable;

it does, however, provide no information on the question what

really happened during the instability in the star. An attempt

was therefore made to calculate the resulting increase in

temperature in the He-shell source. (The computer program used

solves automatically the nonlinear equations).

For this purpose an additional sequence of approximately

600 models was calculated. The changes observed in the star

occur within relatively short periods of time. Therefore, these

models are no longer characterized by their age (after having

left the original main series) but rather their time difference

as compared with the first model of this series (Model 607

of the age $7.9726 \cdot 10^7$ years). Evidently the shell source

is already unstable in several earlier models. (cf. the appendix

on the actual finding of the instability by numerical
difficulties.) During efforts to establish the right size of
the time step, several models with time steps which were too large
for this purpose, were still integrated. This did, however, not
result in considerable changes of the total structure of the
star because the time steps were already very small against
the common time scale of evolution (cf. the high model numbers
towards the end of Table 1). Starting with these models, the
subsequent calculations were therefore carried out with
appropriate time steps instead of searching for the first
unstable model for the time t = 0.

As a whole, the series covers the period from t = 0 to
t = 23200 years. The events in the star for this period of time
are represented in Figs. 5 and 7. In Tables 4 and 5 the inner
models for t = 18000 and t = 19070 years are represented.

At the time t = 0 the star has a luminosity of $\lg\frac{L}{L_\odot} = 4.310$;
it is produced almost entirely in the H-shell source at $M_r/M = 0.1603$
(thicknes $\Delta M_r/M \simeq 10^{-5}$). The He-shell source contributes only
7%; its maximum ε is at $M_r/M = 0.1597$ at a temperature of
$\lg T = 8.222$.

The initial increase in temperature in the He-shell source
is with $T/T = 4 \cdot 10^{-12}$ sec^{-1} rather slow; it becomes, however,

faster and faster. After 320 years the greatest velocity
has been reached with $\tilde{T}/T = 2 \cdot 10^{-10}$ sec^{-1}.

Due to the increas in temperature the energy production
during this period of time increases very strongly. This
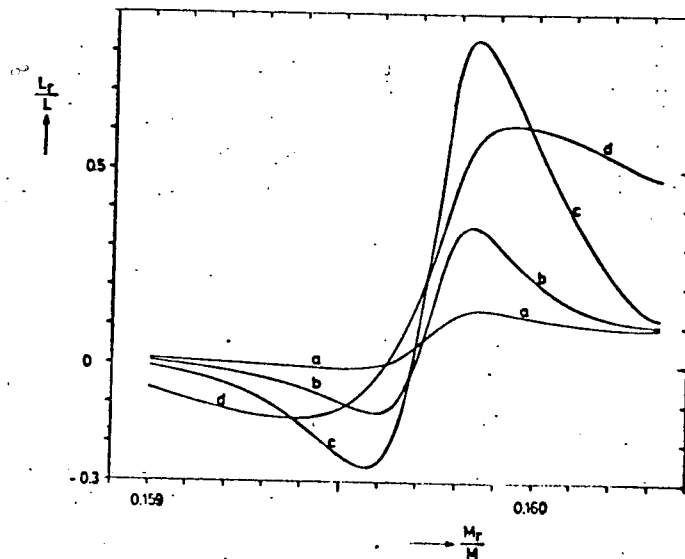results in a strong increase of L_r in the region of the He-shell
source.

Figure 4. The course of L_r/L in the Helium-shell source (to the
right up to the beginning of the hydrogen shell source) in several
models during the first thermal pulses. The models are for the
times t = 289 (a), t = 321 (b), t = 337 (c), and t = 385 years (d).

In Fig. 4 L_r/L is plotted as a function of M_r/M for

several models. One can see that a maximum of L_r/L is formed

and increases rapidly. Above this maximum the luminosity is again

absorbed by work of expansion and by the increase in inner

energy. Thus the luminosity increases only very slowly above

the shell source, i.e. in the stable region). In the lower

part of the shell source, not far from the point with maximum ϵ_{He},

the following applies $L_r < 0$, because here, ϵ_{He} is very small

(since Y is small), much smaller than the value of ϵ_g which

here, like in the entire shell source, is negative. Thus, energy

is distributed to both sides of the maximum of the shell source

(maximum of temperature). The maximum of luminosity within the

He-shell source shows greater and greater values up to $t \doteq 337$ years

(up to $L_r = 0.83$ L), while the side minimum with $L_r = -0.26L$

decreases simultaneously to its lowest value.

With the increase in luminosity a convective ring began

to form at t = 320 years in the upper part of the He-shell source.

This convective ring grew rapidly upwards and downwards and

covered maximally the range $M_r/M = 0.15976$ to 0.10017 (cf.
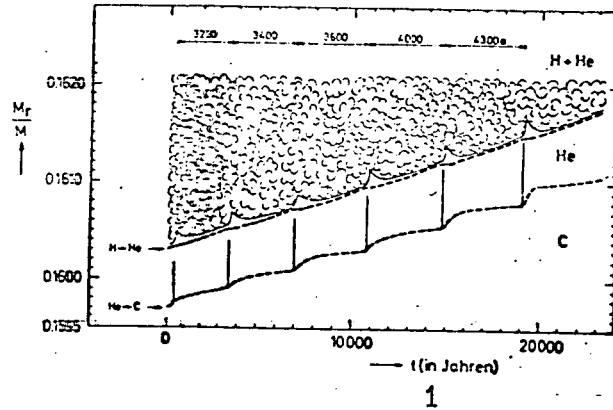
Fig. 5 and 6).

$\mathcal{E}$

Figure 5. M_r-t-Diagram for the region around the two shell
sources during the thermal pulses of the He-shell source.
In both sources the points of maximum energy production are
dashed. The "cloudy" region corresponds to the outer convective
zone. The convective regions which occur during each of the
6 pulses between the shell sources are of such short duration
that they could only be indicated here by vertical straight
lines. In the upper portion of the graph the time intervalls
between consecutive maxima are indicated.

1 t (in years)

After the maximum L_r in the He-shell source decreases again slowly but a steadily increasing portion of it is transferred to the outside (Fig. 4). The contribution of the H-shell source decreases simultaneously. During approximately 2500 years the temperature in the He-shell source decreases again to the original value whereby this region also contracts again (cf. the curves for lgT and lgρ in Fig. 7). At t = 3000 years the original state (like at t = 0) has in essence been reached again. The He-shell source is again thermally unstable, the temperature in it approaches a new maximum, etc. .
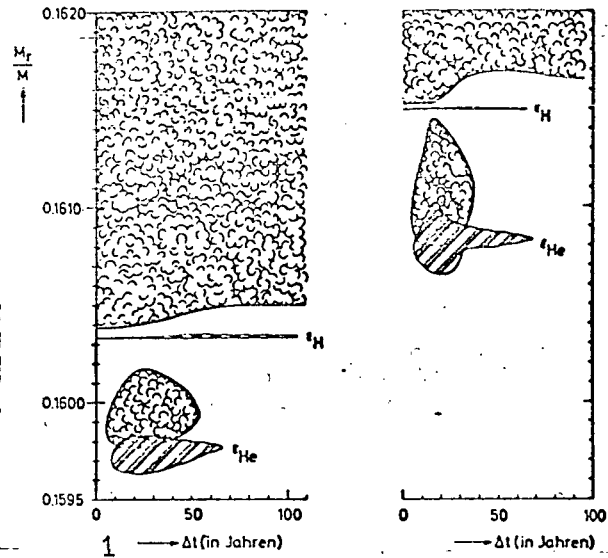
Figure 6. M_r-t-Diagram for the 1. (left) and the 6. thermal pulse (right). The scales are considerably expanded as compared with those in Fig. 5 (the time Δt starts from arbitratily chosen zero points). "Cloudy" regions correspond to convective zones. Densely shaded are the regions in which the nuclear energy production ϵ was greater than $10^{7.5}$ erg $\cdot$ g^{-1} sec^{-1}.

1 Δt (in years)

The local instability in this model is thus not unique:
the resulting increase in temperature repeats itself in the
form of cyclicly recurring thermal pulses in the He-shell
source. The duration of these "cycles" is approximately
some 10^3 years. It grows (calculated from maximum to maximum)
from 3200 to 4200 years (Fig. 5).

The calculations have shown that the pulses are similar
among themselves. However, they do not reproduce each other
exactly. Thus, a total of 6 cycles was finally calculated.
What is repeated again and again, is the fast "running up"
of the temperature in the He-shell source during the instability
(within a period of some 10^2 years), which is followed by the
much smaller decrease (over some 10^3 years). For comparison,
the Kelvin-Helmholtz time scale τ for the initial model
(t = 0) may be given: for the entire star $\tau = 4 \cdot 10^4$ years,
for the region of the helium shell source $\tau = 10^3$ years.

The thermal pulses become, however, each time stronger,
i.e. the difference between the models in the maximum and the
minimum, respectively, become greater and greater. This is
clearly demonstrated in Fig. 7 which gives an impression of
the changes of several parameters during the entire period of
time covered by the calculations. The amplitude of the

temperature in the He-shell source increases slowly (from

$\Delta \lg T = 0.13$ to $\Delta \lg T = 0.24$, Fig. 7a), the minima become

lower and lower, the maxima greater and greater. Since ϵ_{He}

changes with a high power of the temperature, the peak of the

luminosity in the shell source increases correspondingly more

strongly each time (from $\frac{L_{Max}}{L} = 0.83$ to $\frac{L_{Max}}{L} = 7$, cf. the

dashed curve in Fig. 7c).
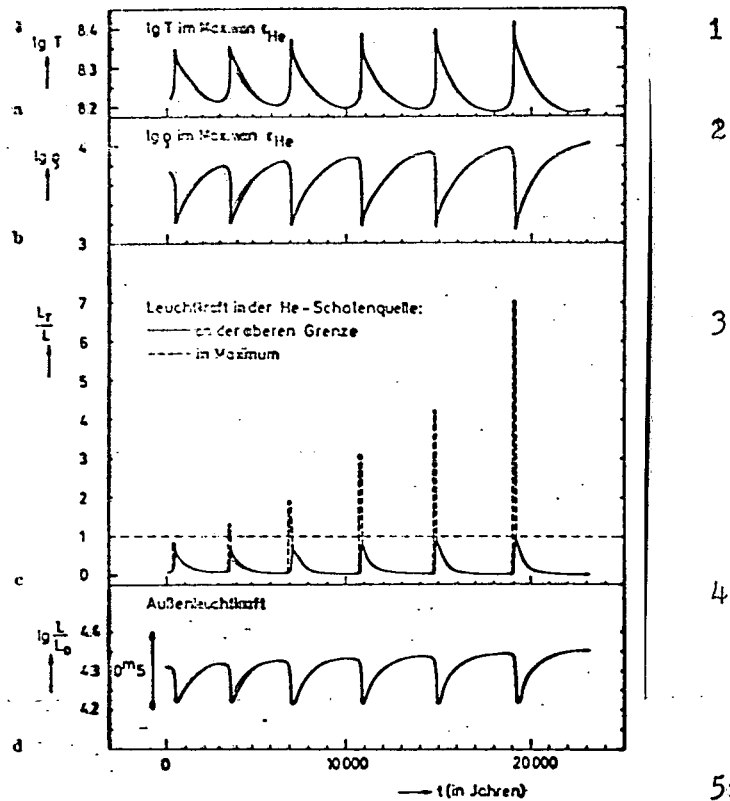
Figures 7a-d. The change in dependence of time of several

important parameters in the star during the thermal pulses of the

He-shell source.

1 lg T at the maximum of ϵ_{He}; 2 lg ρ at the maximum of ϵ_{He}

3 luminosity in the He-shell source: —— at the upper boundary

---- at the maximum; 4 outside luminosity; 5 t (in years)

With the constantly increasing maximum of the luminosity
the expansion of the convective zone above the He-shell
sources increases also (cf. Fig. 5 and 6). Most significantly,
this convection approaches more and more the hydrogen-rich
region from which, during the 6. maximum, it is only
separated by a mass region of $\Delta M_r = 5 \cdot 10^{-5} M_\odot$. The difference
in pressure between the upper edge of the convective zone
and the hydrogen-rich region, however, with $\Delta \lg P = 0.9$
amounts then still to 2 scale heights. Thus, there is as yet
no danger that, for instance, by "overshooting" convective
elements, hydrogen might be mixed into the hot regions of the
He-source (cf. the previous chapter). This may, however,
happen later, should the pulses continue to increase. For
the time being, the difference in pressure, $\Delta \lg P$, in question,
decreases from maximum to maximum by approximately 0.1.
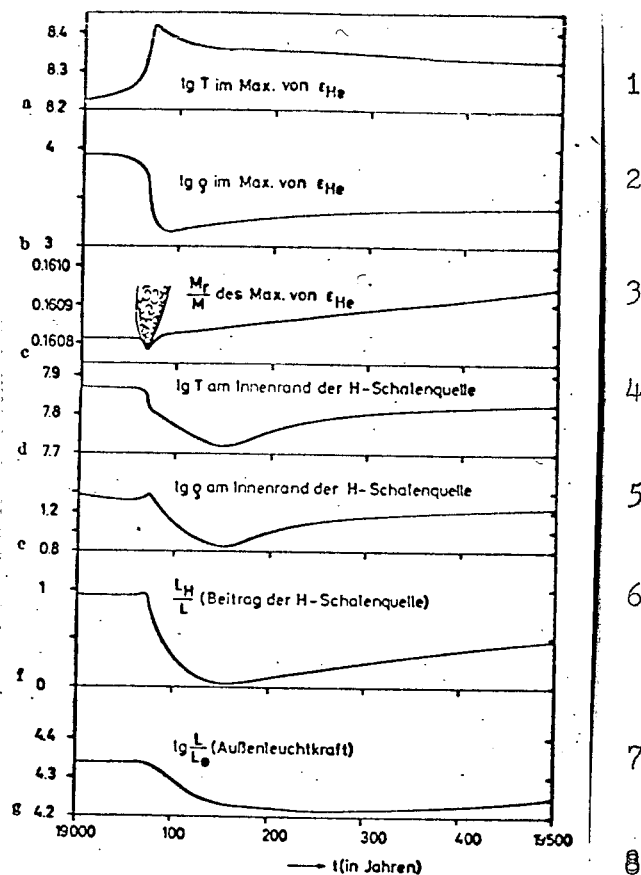
Figures 8a - g. The change in dependence of time of several

functions in the two shell sources and the outside luminosity

during the 6. thermal pulse (the time scale is strongly expanded

as compared with that of Fig. 7).

1 lg T at the maximum of ϵ_{He}; 2 lg ρ at the maximum of ϵ_{He};
3 $\frac{M_r}{M}$ at the maximum of ϵ_{He}; 4 lg T at the inner boundary of the
H-shell source; 5 lg ρ at the inner boundary of the H-shell source;
6 $\frac{L_H}{L}$ (contribution of the H-shell source); 7 lg $\frac{L}{L_\odot}$ (outside
luminosity; 8 t (in years).

These convective zones are always temporarily present. Their influence on the helium distribution can be seen in Fig. 9: the helium content Y over the mass is represented for the minima of temperature before the first, second, and third pulse (curves 1 - 3), as well as during and after the 6. pulse (curves 6a, b, c). Initially (curve 1) a completely smooth curve is observed up to the steep decrease to the right which, in the H-shell source, progresses to the low helium content in the outer regions (Y = 0.4). A considerable portion of the entire helium consumption takes always place in short periods of time at maximum ϵ_{He}. Then, however, convection is always present and the high helium consumption is distributed over a larger region. Thus, the relatively flat plateaus in the latter curves of Fig. 9 are formed in the direction of Y. The steep increase following the plateaus to the right (for instance at M_r = 0.16115 M for curve 6a) shows, how far the convection of the preceding maximum reached to the outside.

The changes in outside luminosity and the contribution of the H-shell source increase also from pulse to pulse. The contribution of the H-shell source to the outside luminosity can be seen from Fig. 7c, namely as a difference of the solid curve (i.e. the luminosity of the He-shell source which is transferred to the outside) to the curve $L_r/L = 1$. This

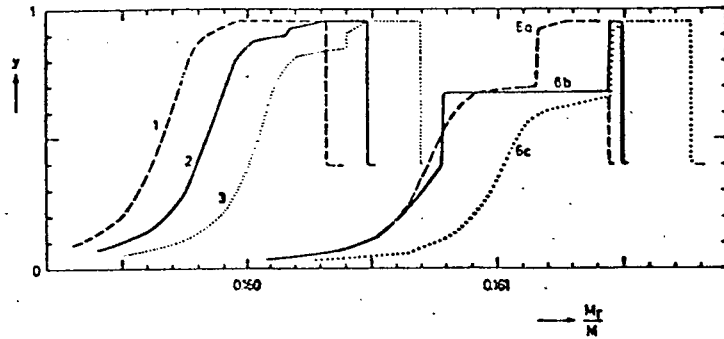Figure 9. The distribution of the helium content Y in the mass
region of the He-shell source in different models. Curves 1, 2,
3, and 6a correspond to models in the minimum before the 1st,
2nd, 3rd, and 6th instability: the curves 6b and 6c correspond
to models during or after the 6th instability. The He-shell
source is always in the steep decrease of the curve (right)
to the helium content of the outer regions.

contribution decreases during the 6th instability from
approximately 95% to 3%. With the decrease in energy production
of the H-shell source the outside luminosity decreases also each
time whereby the amplitude increases from $\Delta \lg L = 0.08$ to
$\Delta \lg L = 0.12$ (Fig. 7d).

The decrease in outside luminosity is associated with the
decrease of the outer radius of the star: during the 6th thermal
pulse we observe that $\Delta \lg R = -0.12$ and that the simulteneous
minor increase in effective temperature ($\Delta \lg T_e = 0.03$) is
overcompensated. The distances of the centers of different
mass elements of the 6th pulse are presented in Fig. 10 as
function of time. In order to maintain hydrostatic equilibrium
(during the occurring changes in pressure) quite different
radial movements are forced upon different regions of the star.
The carbon core below the He-shel source behaves practically
like a solid sphere (cf. the curve for $M_r/M = 0.16008$ in Fig.10).
Strong expansion during the instability is naturally experienced
by the region of the He-shell source itself the relative
extension of which has been approximately doubled (cf. in Fig. 10
the area between the dashed curves which gave the maxima of ϵ_{He}
and ϵ_H). The greater proportion of this expansion takes place
after the time of maximum energy production in the He-shell source
($t = 19070$ years), namely then when the energy production in this

Table 4. The model for t = 18000 years. In the convective region log T is printed in italics

M_r/M	$\log P$	$\log T$	$\log r$	L_r/L	X	Y	$\log \varrho$
0.97103	3.933	*4.036*	13.564	1.000	0.556	0.400	—8.185
0.90530	4.510	*4.263*	13.509	1.000	0.556	0.400	—7.837
0.80189	4.959	*4.436*	13.444	1.000	0.556	0.400	—7.564
0.70669	5.238	*4.543*	13.388	1.000	0.556	0.400	—7.394
0.60642	5.478	*4.632*	13.328	1.000	0.556	0.400	—7.247
0.50580	5.695	*4.712*	13.260	1.000	0.556	0.400	—7.113
0.39659	5.931	*4.798*	13.167	1.001	0.556	0.400	—6.966
0.27109	6.270	*4.917*	12.993	1.001	0.556	0.400	—6.754
0.16460	7.922	*5.445*	12.065	1.002	0.556	0.400	—5.691
0.16223	9.281	*5.836*	11.526	1.002	0.556	0.400	—4.783
0.16175	10.532	*6.177*	11.091	1.002	0.556	0.400	—3.930
0.16158	11.676	*6.480*	10.718	1.002	0.556	0.400	—3.139
0.16150	12.904	*6.801*	10.333	1.002	0.556	0.400	—2.282
0.16146	14.199	*7.136*	9.939	1.002	0.556	0.400	—1.369
0.16143	15.633	7.501	9.514	1.001*	0.556	0.400	—0.341
0.16142	16.874	7.814	9.167	0.942	0.549	0.407	0.579
0.16141	17.006	7.843	9.133	0.806	0.495	0.461	0.722
0.16141	17.098	7.860	9.113	0.593	0.367	0.589	0.887
0.16141	17.178	7.869	9.099	0.323	0.247	0.709	1.064
0.16141	17.265	7.872	9.088	0.043	0.021	0.935	1.343
0.16140	17.892	7.888	9.045	0.039	0.000	0.956	2.157
0.16116	19.387	8.094	8.959	0.034	0.000	0.926	3.493
0.16115	19.399	8.096	8.958	0.034	0.000	0.708	3.524
0.16081	19.876	8.184	8.926	0.029	0.000	0.593	3.921
0.16074	19.946	8.195	8.921	0.026	0.000	0.429	3.996
0.16067	20.000	8.203	8.917	0.024	0.000	0.293	4.056
0.16058	20.069	8.212	8.913	0.022	0.000	0.174	4.127
0.15914	20.659	8.284	8.872	0.012	0.000	0.010	4.635
0.14809	21.748	8.325	8.775	—0.003	0.000	0.000	5.500
0.12211	22.474	8.272	8.678	—0.006	0.000	0.000	6.013
0.07584	23.076	8.170	8.541	—0.004	0.000	0.000	6.420
0.03807	23.418	8.086	8.398	—0.001	0.000	0.000	6.651
0.01463	23.624	8.036	8.232	—0.000	0.000	0.000	6.792
0.00000	23.815	8.000	1.000	0.000	0.000	0.000	6.923

source has already decreased considerably and the pressure decreases also.

The envelopes immediately above the He-shell source (curves for M_r/M = 0.16150 to 0.16152) show also strong relativ changes in radii. These mass elements are located in the very steep decrease in pressure which follows the H-shell source to the outside (before the instability, $-\frac{\partial P}{\partial M}$ is here 10^{16} times as great as for M_r = 0.5 M; cf. the model for t = 18000 years in Table 4).

The initial flat decrease of these log r-curves (up to about t = 19070 years) is solely brought about by the outside burning of the H-shell source; in the course of this event the steep decrease in pressure is shifted to mass shells which are located somewhat further outside. There the pressure increases therefore strongly and is compensated by contraction. These layers contract very strongly after t = 19070 while the regions below expand. During this time the zero point of the change in pressure is in the H-shell source between $\dot{P} < 0$ on the inside and $\dot{P} > 0$ on the outside. Accordingly, the intersection of $\dot{r}$ is somewhat above the H-shell source. If, approximately 10 years later, the energy production of the H-shell source has decreased to about one half of the original value, it ceases to be the intersection of $\dot{P}$.
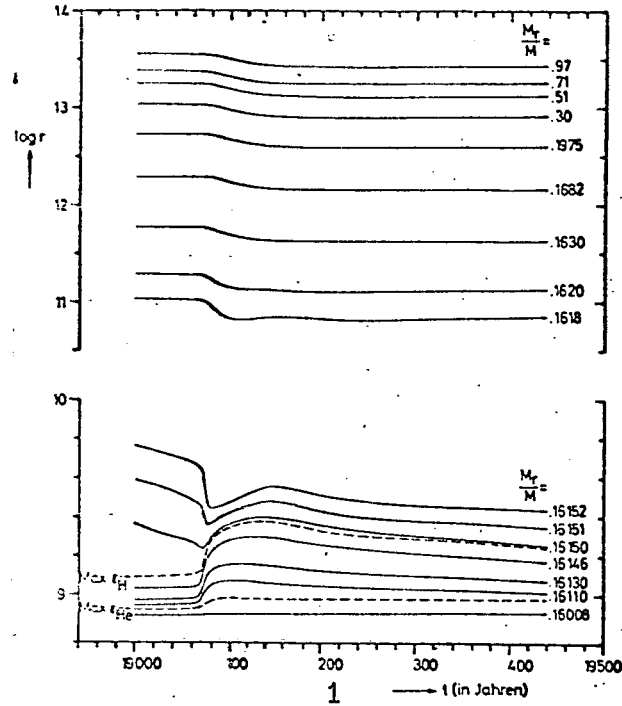
Figure 10. The change in dependence of time of the radius
(r in cm) of individual mass shells (the M_r/M-values are given)
during the 6th thermal pulse. The location of the maximum
of both shell sources is shown in a dotted curve (it should
be observed that the lower log r-scale for the region of the
shell source as opposed to the upper scale for the outer
layers is expanded by a factor of 2)

1 t (in years)

The zero point of $\dot{P}$ moves further to the outside thus shifting
the zero point of $\dot{r}$ to the region outside of the steep decrease
in pressure (cf. the analogous behavior of the models during
central helium-burning and for the first exhaustion of the
H-shell source as described in the "reflection principle" for
the change of the functions in dependence of time; Hofmeister,
Kippenhahn, Weigert, Stellar Evolution III, 1964). Finally,
all outer layers react only with a slow :contraction as the
pressure rises somewhat in them. This happens when the energy
production of the H-shell source decreases strongly and the
pressure curve above this source becomes considerably flatter.

Without further computations it can not be seen in which
way the thermal pulses of the He-shell source will continue.
It could be that they keep increasing in strength and influence,
for instance ,the overall evolution of the star by strong mixing,
or else, finall become constant and are only overlapping,
temporary, and insignificant interludes of "normal" evolution.
It is as yet not even clear what in essence produces the
intensifying effect of the pulses which have been observed
thus far. If one, for instance, compares two models of consecutive
minima, one then finds that during the pulse the patterns of
almost all functions have shifted somewhat. It is possible that

the reason will be found in the slow changes in the models

during normal evolution. The influence of preceding pulses

on subsequent ones can only take place by way of the described

changes in the helium distribution (by the brief convection

in the He-shell source). At the maximum of ϵ_{He} Y is temporarely

increased by convection (cf. the curves 6a and 6b in Fig. 9),

the relative increase in Y is greater each time. The increase

in ϵ_{He}, thus brought about, is of the order of magnitude of a

factor of 2 for the 6th instability. Otherwise this convection

has naturally a damping effect due to its very effective transport

of energy.

It is easier to understand why a pulse is discontinued

and a new one begins. It is evident from the discussion of

Schwarzschild and Härm that the instability must become weaker

and weaker with increasing relative expansion of the He-shell

source; now the energy produced in excess is utilized more and

more to perform work of expansion and to a lesser and lesser

extent to increase the inner energy. We find this situation

with each occurrence of the "running up" of the temperature to a

maximum. The quotient $\frac{\dot{T}/T}{\dot{\rho}\rho}$ for the maximum of ϵ_{He} is a measure

for the ratio of the increase in inner energy to the work of

expansion performed. At the beginning of the 6th pulse at

$t = 19060$ a it is -0.67 ($\dot{\rho}/\rho < 0$, $\dot{T}/T > 0$). The value decreases

Table 5. The model for t = 19070 years. In the convective regions
log T is printed in italics.

M_r/M	$\log P$	$\log T$	$\log r$	L_r/L	X	Y	$\log \varrho$
0.97103	3.903	*4.072*	13.554	1.000	0.556	0.400	—8.161
0.90530	4.545	*4.271*	13.499	1.000	0.556	0.400	—7.809
0.80189	4.997	*4.497*	13.434	0.998	0.556	0.400	—7.536
0.70669	5.276	*4.552*	13.379	0.997	0.556	0.400	—7.365
0.60642	5.517	*4.632*	13.318	0.995	0.556	0.400	—7.218
0.50580	5.734	*4.722*	13.250	0.993	0.556	0.400	—7.084
0.39659	5.970	*4.807*	13.157	0.990	0.556	0.400	—6.937
0.27109	6.310	*4.935*	12.983	0.985	0.556	0.400	—6.725
0.16468	7.963	*5.455*	12.054	0.979	0.556	0.400	—5.660
0.16231	9.329	*5.834*	11.513	0.979	0.556	0.400	—4.748
0.16183	10.593	*6.192*	11.074	0.978	0.556	0.400	—3.886
0.16166	11.761	*6.502*	10.694	0.978	0.556	0.400	—3.078
0.16158	13.035	*6.835*	10.295	0.978	0.556	0.400	—2.188
0.16154	14.412	*7.193*	9.878	0.978	0.556	0.400	—1.217
0.16151	15.737	*7.522*	9.496	0.940	0.556	0.400	—0.227
0.16150	16.758	*7.703*	9.236	0.779	0.555	0.400	0.587
0.16150	16.990	*7.817*	9.184	0.541	0.463	0.493	0.847
0.16150	17.075	*7.823*	9.169	0.326	0.348	0.608	1.003
0.16149	17.137	*7.833*	9.160	0.143	0.208	0.748	1.162
0.16149	17.197	*7.834*	9.154	0.026	0.021	0.935	1.367
0.16148	17.664	*7.833*	9.120	0.015	0.000	0.956	1.973
0.16144	18.244	*7.908*	9.087	0.144	0.000	0.922	2.524
0.16144	18.309	*7.930*	9.083	0.199	0.000	0.682	2.590
0.16136	18.724	*8.070*	9.054	0.862	0.000	0.682	2.853
0.16127	19.030	*8.170*	9.028	1.983	0.000	0.682	3.048
0.16121	19.185	*8.219*	9.012	2.918	0.000	0.682	3.148
0.16108	19.410	*8.289*	8.987	4.906	0.000	0.682	3.294
0.16102	19.512	*8.321*	8.975	6.045	0.000	0.682	3.361
0.16092	19.635	*8.358*	8.959	7.018	0.000	0.682	3.440
0.16082	19.758	*8.390*	8.942	3.713	0.000	0.682	3.521
0.16079	19.785	*8.404*	8.938	1.130	0.000	0.682	3.539
0.16079	19.793	8.406	8.937	0.166	0.000	0.523	3.561
0.16078	19.801	8.406	8.936	—0.069	0.000	0.400	3.584
0.16075	19.828	8.401	8.932	—0.530	0.000	0.362	3.629
0.16070	19.880	8.376	8.926	—0.882	0.000	0.299	3.734
0.16055	20.009	8.277	8.914	—0.259	0.000	0.145	4.006
0.15914	20.640	8.259	8.871	0.007	0.000	0.010	4.637
0.15618	21.157	8.317	8.831	0.002	0.000	0.001	5.045
0.14809	21.747	8.322	8.775	—0.005	0.000	0.000	5.501
0.12211	22.475	8.269	8.678	—0.007	0.000	0.000	6.014
0.07584	23.076	8.168	8.541	—0.004	0.000	0.000	6.420
0.03807	23.418	8.084	8.398	—0.001	0.000	0.000	6.651
0.01463	23.624	8.034	8.232	—0.000	0.000	0.000	6.792
0.00000	23.815	7.994	1.000	0.000	0.000	0.000	6.923

with the increasing expansion of the He-shell source; at

t = 19074 a it becomes $\frac{\dot{T}/T}{\dot{\rho}\rho} > 0$, since now the temperature

decreases again upon expansion ($\dot{\rho}/\rho < 0$, $\dot{T}/T < 0$). The

instability ceases actually earlier, namely then when

$\frac{\dot{T}/T}{\dot{\rho}\rho} \approx -0.15$. Despite a continuous increase in temperature the

following applies, $\dot{\epsilon}/\epsilon < 0$: if one expresses the dependence

of energy production ϵ_{He} from ρ and T, as is often done,

with $\epsilon_{He} \sim \rho^2 T^{\nu}$, then one finds the following

$$\frac{\dot{\epsilon}_{He}}{\epsilon_{He}} = 2\frac{\dot{\varrho}}{\varrho} + \nu\frac{\dot{T}}{T} = 2\frac{\dot{\varrho}}{\varrho}\left(1 + \frac{\nu}{2}\frac{\dot{T}/T}{\dot{\varrho}/\varrho}\right), \qquad (9)$$

which is positive for negative $\dot{\rho}/\rho$, as long as $1 + \frac{\nu}{2}\frac{\dot{T}T}{\dot{\rho}\rho} < 0$.

The instability ceases thus because $\frac{\dot{T}/T}{\dot{\rho}\rho}$ becomes smaller and,

besides that, because $\nu = -3 + 43.2/T_8$ which decreases strongly

with increasing temperature (at the beginning of the instability

we find that $\nu = 22$, at the maximum of temperature we find

that $\nu = 13.5$).

As soon as the instability of the He-shell source is over

the models are quite similar to the models before the beginning

of the first instability : during stable burning a relatively

large He-shell source provides practically the entire luminosity;

not far above it, a H-shell source of limited productivity is

to be found. As earlier, this can, however, not be a stationary

state. The He-shell source of large ϵ_{He} and relatively small

energy yield per gram approaches rapidly the H=shell source

of small ϵ_H and high energy yield per gram $\left[\text{cf} \text{ equation (8)} \right]$.

This can be seen clearly in Fig. 5 from the different slopes

of the curves of the two shell sources after each pulse. The

temperature in the H-shell source, and thus ϵ_H, must now again

begin to increase and, correspondingly, ϵ_{He} must decrease.

For the small ϵ_{He} (required for the equal distance between the

two shell sources) which is finally attained the relative

expansion $\dfrac{\Delta r}{r}$ of the He-shell source is, however, again very

small and this shell source thus again thermally unstable. If

the temperature decrease $\dfrac{\ln T}{M_r}$ for the H-shell source remains

in essence unchanged the temperature increase will be approximately.

$$\frac{\dot{T}}{T} = \frac{\partial \ln T}{\partial M_r} \cdot (\dot{M}_H - \dot{M}_{He}) = \frac{\partial \ln T}{\partial M_r} \cdot \left(\frac{L_H}{XE_H} - \frac{L_{He}}{YE_{He}} \right) . \qquad (10)$$

From this we obtain $\dot{T}/T = 4 \cdot 10^{-3} a^{-1}$ for t = 19480. The

corresponding time constant will subsequently become greater

and greater if the change in distance in dependence of time for

the two shell sources $(\dot{M}_H - \dot{M}_{He})$ decreases with increasing

L_H/L_{He}. Here we find the reasons for the relatively long

periods of times of some 10^3 a for the return to instability

(and thus in essence the duration of the entire cycle since the

increase in temperature during instability is of considerably

shorter duration).

In order to repeat the thermal pulses, evidently two
conditions must be fulfilled: firstly, no permanent change must
result from any given pulse (for instance in the chemical
composition in large areas of the star due to mixing);
secondly, another active or potential shell source must be present
before the unstable shell source (thus a region where burnable
constituents are still present but are already exhausted in
inner regions. The difference in time between two instabilities
is in essence given by a (local) nuclear time scale; it is
thus great compared with periods of time which are directly
accessible to observation. One would, however, arrive at
considerably shorter "periods" if the return of the He-shell
source to instability would take place with a local <u>thermal</u>
time scale . This may be expected for models in which the H-shell
source would also be unstable during periods of low energy
production.

The changes during the thermal pulses are rapid compared
with the events normally dealt with in the theory of stellar
evolution. Therefore, the validity of the integrated fundamental
equations has to be checked (cf. Hofmeister, Kippenhahn, Weigert,
Stellar Evolution I, 1964, page 220 ff.). In these equations
the following time scales were assumed to be negligibly small:

the time scales for attaining hydrostatic equilibrium, those
of adiabatic convection, and those of frequencies of the
equilibria of the abundances of the elements participating
in the nuclear reactions. It can be seen from Fig. 10 that
during the 6th pulse the greatest accellerations (illegible) ($\ddot{r}$?)
occur at approximately t = 19070 a. The ratio $\left|\dfrac{\ddot{r}}{g}\right| = \left|\dfrac{\ddot{r}r^2}{GM_r}\right|$ was
estimated from the results of the calculations; it is greatest
in the outer layers (because here $\ddot{r}$ is greatest and M_r/r^2 is
smallest) but always smaller than 10^{-5}. The neglect of the
inertia term in the impuls equation (i.e. the assumption of
hydrostatic equilibrium) is thus justified. - The velocity
of convection changes most rapidly in the temporary convective
shell above the He-shell source. For this location and for
the time of the 6th maximum of L_{He} the following was computed
with the equations of the theory of "mixing length" the fully
developed convection has a very small super-adiabatic gradient

$$\nabla - \nabla_{a\ell} \approx \left(\frac{L_r \nabla_{a\ell}}{\pi r^2\, P\, \sqrt{g\, H_P}}\right)^{2/3} = 7 \cdot 10^{-7}$$

and a mean velocity of approximately

$$v_K \approx \left[\frac{1}{8}\, g\, H_P\, \delta(\nabla - \nabla_{ad})\right]^{1/2} = 10^{-3.65}\, v_S = 3 \cdot 10^4\, \text{cm sec}^{-1}.$$

The life time τ_K for a convective element is approximately
the time during which it passes through one scale height of

pressure $H_p = RT/\beta \mu g = 10^{7.88}$ cm, namely $\tau_K = H_p/v_K = 10^{3.4}$sec.
This should be a good measure for the time required to establish
convection. In view of the small super-adiabatic gradient
the element can be accellerated to full speed during this
period of time and the entire convective shell has only an
extension which is of the order of magnitude of the scale height.
It can thus be assumed that the convection is indeed momentarily
adjusted and adiabatic for the resulting changes in speed.
The shell sources cover only very small mass ranges and nuclear
burning in them takes therefore place at unusually high
temperatures. Typical values for the H-shell source are $\log T = 7.8$,
$\log \rho = 1.$ At the same time, however, the time required for
passing through a full C-N-C-cycle is only of the order of
magnitude of one year. The assumption that the abundances of
the reacting types of nuclei are always equal to the abundances
of equilibria is certainly good.

Appendix: On the Numerical Calculations

Three points shall be briefly discussed here, namely:
a) the treatment of extremely thin shell sources, b) the
selection of the integration steps with regard to space and time
for the fast changes during the instabilities, and c) the discovery
of instabilities by numerical calculations.

a) If a shell source remains active for an extensive period of
time or if the burning begins even in a chemical inhomogenyity

which has been transported to the interior by convection (as for
the hydrogen-shell source in the calculations discussed here)
then the nuclear reactions are restricted to a very narrow
range of masses ΔM_s. Within it, the energy L_s per sec be
produced by reactions which deliver the energy E erg g^{-1}. Then
the local nuclear time scale in the shell source, $\tau_s = \Delta M_s \cdot E/L_s$,
may become small against that with which the actually interesting
changes in the star take place, for instance, small against the
Kelvin-Helmholtz-time scale of the star. According to our
earlier calculation method, irrationally small time steps would
have to be chosen in order to only prevent that the shell
source advances in one time step by more than its diameter.
Instead of that, the time steps Δt were adjusted to the other
changes in the star and the H-shell shifted by the mass
$\Delta M_r = L_H \cdot \Delta t/E_H \cdot X$, whereby ΔM_r may be a multiple of ΔM_s.
More precisely expressed, the smallest positive X-value still
taken into consideration was shifted by this value on the
M_r-scale. The remaining X-values in the shell source were
then shifted in such a way that everywhere in the shell source
the following was valid $\frac{\partial X}{\partial M_r} = -\dot{X} = \epsilon_H/E_H$, whereby ϵ_H was derived
from the latest calculated model and also shifted by ΔM_r. This
method could be incorporated easily into the existing program
and test calculations with $\Delta t < \tau_s$ had shown that such an X-profil
is obtained in good approximation.

Upon such shift of the shell source, a region with great

and spatialy widely different gradients of P and T shifts in

the model. This has to be taken into account for the numerical

formation of the terms $\dot{P}$ and $\dot{T}$ (which are used for the calculation

of $\epsilon_g = -T\frac{\dot{S}}{t}$). For instance, a term of the form $-\frac{P}{M_r} \cdot \frac{\Delta M}{\Delta t}$

makes the greatest contribution to $\dot{P}$. (cf. the detailed discussion

on these points in Hofmeister, Kippenhahn, Weigert, 1966).

b) It is typical for the calculations of local thermal

instabilities (for the flash as well as for the pulses of the

shell source) that in wide regions of the star almost nothing

happens while in a limited region the functions are changing

very rapidly with time and space. What is required here are, on

the one hand, very subtle steps (for instance for the exact

determination of moving boundaries of convective zones); on

the other hand, the limits for doubling the steps or for

reducing them by one half had to be changed constantly with

the changing patterns of the functions. It was soon found to

be most advantageous to bring about a subtle division in space

in the rapidly changing region of the model solely by the

condition $\Delta M_r/M < K$. In the region between the two shell

sources most of the calculations on the instabilities were

carried out with $k = 2.5 \cdot 10^{-4}$.

Particular difficulties were encountered initially with the choice of the size of the time steps during the calculations on the thermal instability. The time steps must be small (about 1/2 year) during the rapid increase in temperature in the He-shell source; they are changing, however, quite considerably for several models. During the automatic time step selection by a built-in sub-program in the computer, it turned out to be advantageous to request a change in maximum luminosity in the He-shell source from model to model by approximately 20%. In this way the result became independent of the time step.

c) Schwarzschild and Härm found the thermal instability of the He-shell source by numerical difficulties during the calculation on the helium-flash. These authors ask in their publication the unsettling question whether one would always observe such, still unknown, instabilities during numerical integrations. There is, naturally, no assurance for that. The sole - however, also absolutely required - approach for that is the repetition of all calculations with altered time steps in order to test the independence of the results from the time step. (This test was always carried out in all of our previous calculations on stellar evolution). Then, however, instabilities would have to be noticed. Indeed, the thermal instability of the He-shell source in the 5 $M_\odot$-star had already been observed numerically

β

when the author received a preprint of the manuscript of
Schwarzschild and Härm. It is undoubtedly a good sign that the
instability appeared and had been noticed immediately and
independently in two numerical calculations with two different
computer programs for quite different stellar models.

Literature

Adams, J.A., M.A. Ruderman, and C.H. Woo: Phys. Rev. 129, 1385 (1963).

Chiu, H.Y.: Phys. Rev. 123, 1040 (1961).

- Neutrinos in Astrophysics. In: Stellar Evolution, p. 175. New York: Plenum Press 1966.

Deinzer, W., and E.E. Salpater: Astrophys. J. 142, 813 (1965).

Hyashi, C., R. Hishi, and D. Sugimoto: Progr. Theoret. Phys. Suppl. 22, (1962).

Hofmeister, E., R. Kippenhahn and A. Weigert: Stellar Evolution I. Z. Astrophys. 59, 215 (1964).

-, -, - Stellar Evolution III. Z. Astrophys. 60, 57 (1964).

-, -, - Methods for Calculating Stellar Evolution; to be published in: Methods in Computational Physics, Vol. 7. New York, London: Academic Press 1966.

Inman, C.L., and M. A. Ruderman: Astrophys. J. 140, 1025 (1964).

Kippenhahn, R., H.-C. Thomas and A. Weigert: Stellar Evolution IV (cited in KTW IV). Z. Astrophys. 61, 241 (1965).

-, -, - Stellar Evolution V (cited in KTW V). In preparation (1966).

Reeves, H.: Nuclear Energy Generation in Stars. In: Stellar Evolution, p. 83. New York: Plenum Press 1966.

- Stellar Energy Sources. In: Stars and Stellar Systems, Vol. VIII, p. 113. Chicago, London: University of Chicago Press 1965.

Schwarzschild, M., and R. Härm: Astrophys. J. 142, 855 (1965).

Unno, W.: Z. Astrophys. 61, 268 (1965).

Weigert, A.: Mitt. astr. Ges. (1965), p. 61.

Zaidi, M.: To be published in: Nuovo cimento, preprint (1965).

Dr. A. Weigert,

University Observatory, 34 Göttingen,

Geismarlandstr. 11